Geometric Optimization of an Impinging Cold-Plate with a Trapezoidal Groove Used for Warm Water Cooling

Yaser Hadad*, Reza Pejman, Bharath Ramakrishnan, Paul R Chiarot, Bahgat G Sammakia
State University of New York at Binghamton
Binghamton, New York, USA, 13850
*Email: yhadad1@binghamton.edu

ABSTRACT

Due to their lower pressure drop, impinging cold-plates are preferred over parallel flow cold-plates when there is no strict space limitation (i.e. when flow can enter perpendicular to the electronic board). Splitting the flow into two branches cuts the flow rate and path in half, which leads to lower pressure drop through the channels. A groove is used to direct the flow exiting the diffuser into the channels. The number of the geometric design parameters of the cold-plate will vary depending on the shape of the groove. In this research, the response surface method (RSM) was used to optimization the fin geometry of an impinging cold-plate with a trapezoidal cross section groove. The cold plate is used for warm water cooling of electronics. Three fin parameters (thickness, height, and gap) and three groove parameters were optimized to reach minimum values for hydraulic and thermal resistances at fixed values of coolant inlet temperature, coolant flow rate, and electronic chip power.

KEY WORDS: Thermal Resistance, Hydraulic Resistance, RSM, Design Parameters, Response Parameters, Regression, Transformation, Normality Assumption, Linearity Assumption, JAYA Algorithm.

NOMENCLATURE

a_{ij}	Constant Coefficients (Eq. (2))
c_p	Specific Thermal Capacity $(J/kg.K)$
f	General Function (Eqs. (1) and (2))
H	Heat Sink Height (m)
h_B	Base Thickness (m)
h_F	Fin Height (m)
h_G	Groove Depth (m)
k	Thermal Conductivity $(W/m.K)$
l_1	Channel Length at the Bottom (m) (Fig. 5)
l_2	Channel Length at the Top (m) (Fig. 5)
m	Counter (Eq. (21))
N	Number of Channels
n	Number of Design Points
P	Pressure (pa)
p	Number of Design Parameters
Q	Heat Sink Volumetric Flow Rate (m^3/s)
q''	Heat Flux (W/m^2)
R_h	Hydraulic Resistance $(1/m.s)$
$\bar{R}_h$	Logarithmic Hydraulic Resistance (Eq. (17))
R_{th}	Thermal Resistance (K/W) or $(K.m^2/W)$
$\bar{R}_{th}$	Logarithmic Thermal Resistance Eq. (16)
Re_{D_h}	Reynolds Number Based on Hydraulic Diameter
T	Temperature (K)
t_F	Fin Thickness (m)
V	Velocity (m/s)
W	Heat Sink Width (m)
w_{Ch}	Channel Width (m) (Fig. 8)
w_h	Weight Factor of Hydraulic Resistance
w_{th}	Weight Factor of Thermal Resistance
w_G	Groove Width at the Top (m)
X_i	General Independent Variable (Eqs. (1), (2))
Y	General Dependent Variable (Eq. (1))
y_G	Groove Width at the Bottom (m) (Fig. 8)

Greek symbols

α	Design Parameter (Table 3)
β	Design Parameter (Table 3)
γ	Design Parameter (Table 3)
δ	Design Parameter (Table 3)
ε	Surface Error of Fitting (Eqs. (1), (2))
θ	Fin Tilt Angle (Fig. 5)
λ	h_B/H (Eq. (10))
μ	Absolute Viscosity $(kg/m.s)$
Ξ	Objective Function (Eq. (20))
ρ	Density (kg/m^3)
σ	Design Parameter (Table 3)
φ	Design Parameter (Table 3)
ω	W/w_{Ch} (Eq. 11)

Subscripts

f	Fluid
s	Solid

INTRODUCTION

DOE (design of experiments) methods associated with different optimization algorithms have been used for optimization of air and water cooled heat sinks extensively. Subasi et al. [1] used RSM and the Pareto based multi-objective optimization to calculate the design parameters optimal values to maximize Nusselt number and minimize friction factor of a honeycomb heat sink. Rao et al. [2] used RSM for the dimensional optimization of a liquid cooling micro-channel heat sink. They minimized thermal resistance and pumping power using the JAYA algorithm and compared their results with the results of other algorithms: MOEA and TELBO. The

grey-based fuzzy algorithm with Taguchi experimental design method were employed by Chou et al. [3] for designing parameter optimization of a parallel plain fin heat sink. Chiang et al. [4] used RSM to estimate the influence of design parameters on the thermal performance and pressure drop of a pin-fin heat sink working with air. Sequential approximation optimization (SAO) was utilized for finding the optimal values of design parameters in their study. Kulkarni et al. [5] optimized a double-layered heat sink working with water for thermal resistance and pumping power using a multi-objective genetic algorithm. Two geometric parameters of channel cross section and the ratio of flow rates in the upper and lower channels were considered as the design parameters. Computational fluid dynamics (CFD) was used to calculate the response parameters and RSM was applied to reduce the computational time. Maximum temperature of a parallel plain fin heat sink was minimized numerically by Taguchi method and the analysis of variance (ANOVA) in [6]. Yang et al. [7] optimized an impinging pin-fin heat sink numerically for stationary and rotating states. RSM and a genetic algorithm method were employed for optimizing the stationary and rotating Nusselt numbers. Manivannan et al. [8] used Taguchi-based grey relational analysis in order to optimize a flat plate heat sink numerically. In their geometric optimization their response parameters were electromagnetic emitted radiation, thermal resistance, average convective heat transfer coefficient, pressure drop and mass of the heat sink. Lin et al. [9] optimized the geometric parameters of a water-cooled, silicon based double layer micro-channel heat sink to minimize the thermal resistance. They calculated optimal values of design parameters at specified values of pressure drop, pumping power and water flow rate. The effects of geometrical and flow parameters on heat transfer and pressure drop characteristics in a water-cooled mini-channel heat sink was studied by Xie et al. [10]. They verified their results by conducting an extra numerical simulation based on an orthogonal DOE Method.

The aim of this study is to develop an optimization approach to obtain the optimal design of an impinging water-cooled cold-plate to facilitate high performance computing (HPC). It is typically used in low profile chassis blade servers with minimum power densities of $300\,W/server$. Six design parameters covering the geometry of the cold-plate (e.g. channels, groove, etc.) are optimized to reach the minimum thermal and hydraulic resistances at fixed chip heat flux, coolant volumetric flow rate and inlet temperature. The current optimization procedure and its final results are expected to provide a guide for the practical design of impinging water cooled cold-plates.

RESPONSE SURFACE METHODOLOGY

The response surface methodology is a collection of mathematical and statistical techniques used for analyzing problems in which design parameters influence response parameters. The goal is to discover the optimal values of the design parameters to achieve the desired value of the response parameters [11]. The RSM and regression analysis allow the response parameters to be obtained as functions of the design parameters. The general form of this function may be represented as:

$$Y = f(X_1, X_2, \ldots, X_p) \pm \varepsilon \tag{1}$$

where Y is the response parameter, f is the regression relation (response surface), X_i $(i = 1, 2, \ldots, p)$ are independent design parameters, ε is the surface error of fitting and p is the number of design parameters. Here, a second order polynomial regression function (quadratic form) is used for approximating f:

$$f = a_0 + \sum_{i=1}^{p} a_i X_i + \sum_{i=1}^{p} a_{ii} X_i^2 + \sum_{i<j}^{p} a_{ij} X_i X_j + \varepsilon \tag{2}$$

where a_0 represents the intercept, and a_i, a_{ii} and a_{ij} are the linear, second order and interaction (mixed terms) coefficients, respectively.

The optimization process can be summarized by the following steps:

1. Identify the fixed, design and response parameters.
2. Use RSM with faced centered central composite design (FCCCD) to obtain the experimental design.
3. Use computational fluid dynamics (CFD) to calculate the values of the response parameters at each permutation of the design parameters identified by RSM.
4. Apply regression analysis to obtain the quadratic functional forms (response surface).
5. Calculate the analysis of variance (ANOVA) for the design parameters to illustrate how much the response parameters are affected by them.
6. Validate the regression function statistically and by modeling intermediate points.
7. Define an objective function based on the response parameters and assign weight factors according to the designer's priorities.
8. Find the optimum designs for the assigned weight factors using JAYA algorithm.

COLD-PLATE GEOMTERY

The geometry of the cold-plate can be divided to three parts: distributor, metal part and collector.

Distributor

The distributor is made of plastic and consists of a short inlet entrance pipe, a curved diffuser (by 90°) and a duct that connects the entrance pipe to the diffuser. The diffuser has a rectangular cross section and supplies the coolant (water) to the micro-channels. It also has two blades for dividing the flow into three paths (Fig.1).

Metal Part

The metal part of the cold-plate is copper and consists of almost 100 channels connected by a longitude groove with a nearly trapezoidal cross section. A schematic of the metal part is shown in Fig. 2 with an exaggeration in the fin thickness and channel width. As seen in Fig. 2, the fins are tilted.

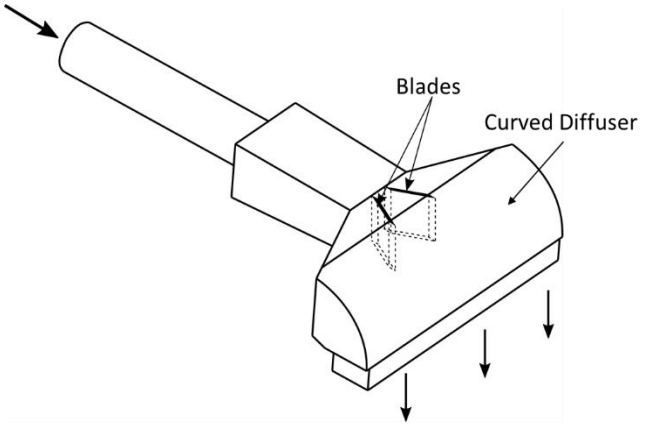

Fig. 1 Distributor

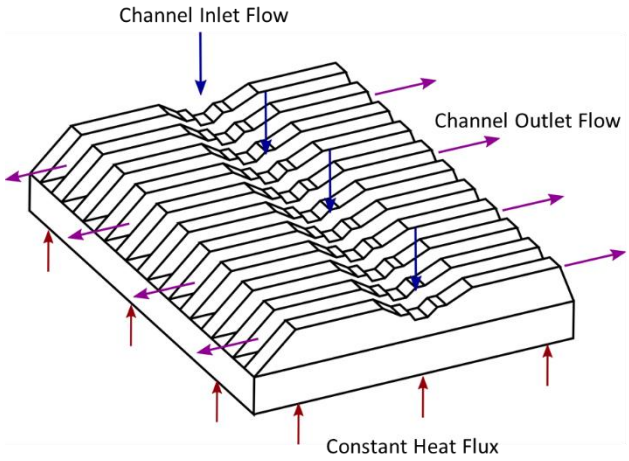

Fig. 2 Metal Part of the Baseline

Collector

The coolant flow is directed to a miniature reservoir from the exit of the channels by two ducts. A circular cross section duct then carries the flow from the reservoir to the exit hose (Fig. 3).

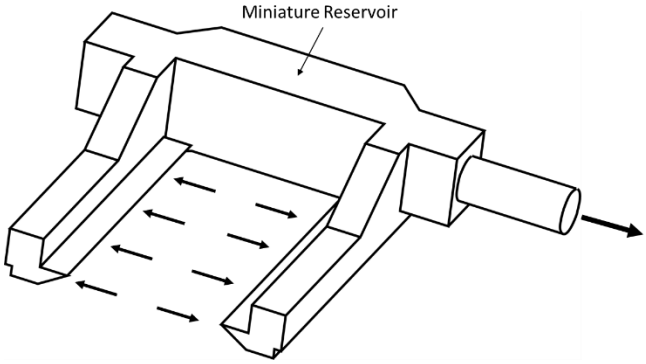

Fig. 3 Collector

Fig. 4 shows a schematic exploded view of the whole package including distributor, metal part and collector. The cover on the top of the channels and fins has not been shown for clarity.

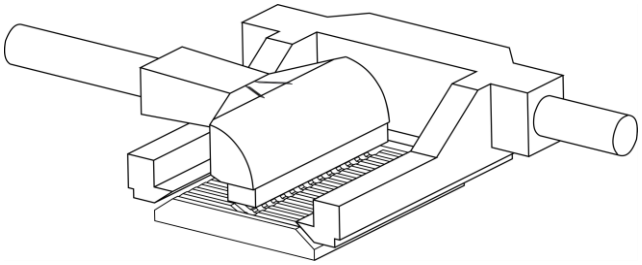
Fig. 4 Cold-Plate Package Exploded View

NUMERICAL ANALYSIS

Basic Assumptions

The following assumptions are made in both the flow and thermal characteristics of the model:

1. The flow is 3-D, steady state, laminar (low Reynolds number in channels) and incompressible.
2. The effects of gravity and any other kind of body force are negligible.
3. The kinematic properties of the coolant and thermal properties of the coolant and solid are constant.
4. Viscous heating and radiation heat transfer are neglected.
5. All channels are identical both in thermal performance and fluid flow. Therefore, the computational domain can be considered as one-half of a unit cell of a micro-channel array (Fig. 5).

Governing Equations

The governing equations for a conjugate (conduction-convection) heat transfer problem in the incompressible steady state laminar flow regime can be written as follows:

Conservation of mass for liquid phase (coolant)

$$\nabla.\vec{V} = 0 \tag{3}$$

Equation of motion for liquid phase (coolant)

$$\rho_f(\vec{V}.\nabla)\vec{V} = -\nabla P + \mu_f\nabla^2\vec{V} \tag{4}$$

Energy equation for liquid phase (coolant)

$$\rho_f c_{p,f}(\vec{V}.\nabla)T_f = k_f\nabla^2 T_f \tag{5}$$

Energy equation for solid phase (metal)

$$k_s\nabla^2 T_s = 0 \tag{6}$$

Numerical Domain and Boundary Conditions

According to the fifth basic assumption, the computational domain is considered one half of a unit cell of a micro-channel array. Fig. 5 shows the computational domain of the baseline (manufactured cold-plate) with associated geometric parameters and boundary conditions. The cell is cut in the middle of the fin thickness so periodic boundary conditions were applied to its sides. Water enters from the top of the groove and after a 90° change in its direction goes through the

channels. A constant pressure drop boundary condition is applied at the exit of the channels. A symmetry boundary condition is used for the front plane of the cell (where the flow splits into branches) because the metal part is symmetric. A constant heat flux boundary condition is applied to the bottom of the cell and simulates the heat generated by an

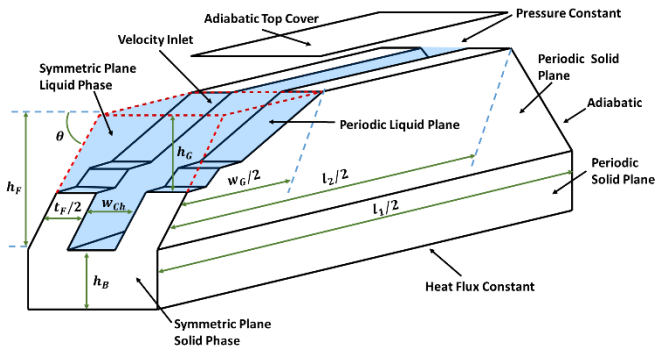

Fig. 5 Computational Domain

electrical chip. The values of the geometric parameters of the baseline are shown in Table 1 for quick reference.

Table 1. Baseline Geometric Parameters in Millimeters

l_1	l_2	w_{Ch}	h_F	t_F	h_B	θ	h_G	w_G	W	N
23.6	18	0.167	2	0.100	1.35	65°	0.8	4	27	100

Numerical Methods

The finite volume SIMPLEC algorithm with pressure based solver was used to solve the governing equations numerically. Second order upwind scheme was employed to discretize the equations of motion and energy. A structured grid with prismatic cells in the groove and hexahedral cells for the rest of the domain (channel and solid phase) was generated for the baseline. A grid sensitivity study was performed based on both the hydraulic and thermal resistances (response parameters).

Coolant and Metal Properties

For conjugate heat transfer problems, in addition to the thermal and kinematic properties of the fluid, the thermal properties of the solid phase should be involved. In the present study, the coolant and solid phase are pure water and copper at room temperature (27°C). The thermal and kinematic properties of the coolant are constant and read from thermodynamics tables at the inlet temperature. The thermal properties of copper at room temperature were applied to the model for the solid phase. Table 2 shows the thermal and kinematic properties of the coolant and thermal properties of the solid phase.

Table 2. Liquid and Solid Phases Properties at 300 K

	c_p $(J/kg.K)$	k $(W/m.K)$	ρ (kg/m^3)	μ $(kg/m.s)$
Coolant	4179	0.613	997	0.000855
Copper	381	388	8978	.....

Validation of the Numerical Model

The simulated pressure drop versus coolant flow rate was validated by comparison with a theoretical model reported in [12]. Fig. 6 illustrates this comparison. The average and maximum difference between the numerical and theoretical results are almost 16% and 17%, respectively.

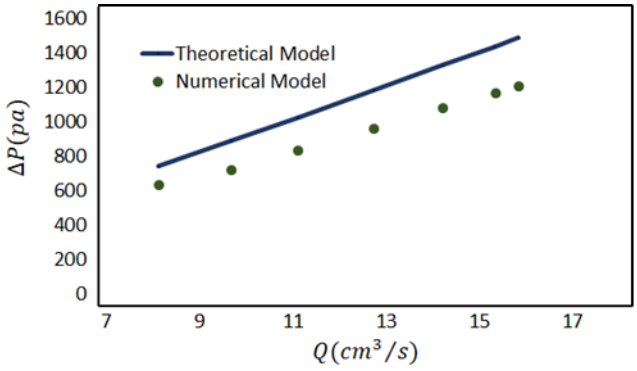

Fig. 6 Pressure Drop vs Coolant Flow Rate

It should be noted that the theoretical model has been solved for channels with a rectangular cross section and extending it to the impinging channels with parallelogram cross section may decrease its accuracy.

For the thermal resistance, the results of the numerical model were compared with the available commercial data released by manufacturer [13] in Fig. 7. For these results, the average and maximum differences are less than 8% and 10%, respectively.

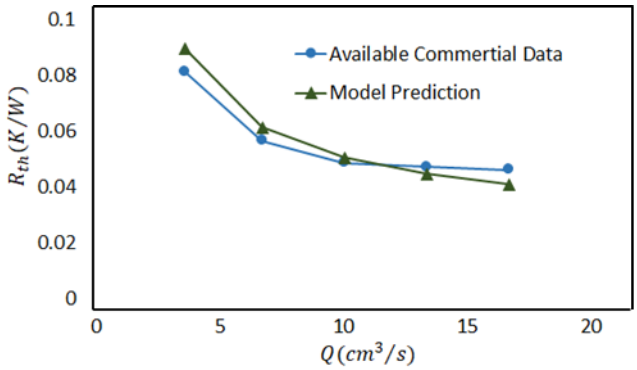

Fig. 7 Thermal Resistance vs Coolant Flow Rate

OPTIMIZATION PROCESS

Fixed Parameters

The optimization study has been performed for constant values of heat flux (chip electrical power and area) and coolant flow rate and inlet temperature. Among the geometric parameters, the base thickness and the width of the cold-plate (h_B and W) as well as the length of the channels (l_1 and l_2) were equated to the values of the baseline (Table 1). Tilt angle of the fins is another parameter that was assumed to be fixed. Although for the baseline the fins are tilted (Fig. 2), in the optimization process they were assumed to be vertical according to [14] which shows $\theta = 90^\circ$ (vertical fins) is the optimum value for both thermal and hydraulic resistances in

short heat exchangers. In the current study the optimization was done for constant heat flux of $257525\ W/m^2$ and coolant flow rate and inlet temperature of $1\ lit/min$ $(16.67\ cm^3/s)$ and $300\ K$, respectively.

Design Parameter

Fin thickness (t_F), fin height (h_F), channel width (w_{Ch}), groove width at the top (w_G), groove width at the bottom (y_G), and groove depth (h_G) are the initial design parameters. Fig. 8 summarizes the initial design parameters. The total height of the plate (H) and the number of channels (N) could be calculated by the following relations:

$$h_B + h_F = H \tag{7}$$

$$Nw_{Ch} + (N-1)t_F = W \tag{8}$$

or

$$N = \left\lceil \frac{W + t_F}{w_{Ch} + t_F} \right\rceil \tag{9}$$

where the brackets denote the ceiling function.

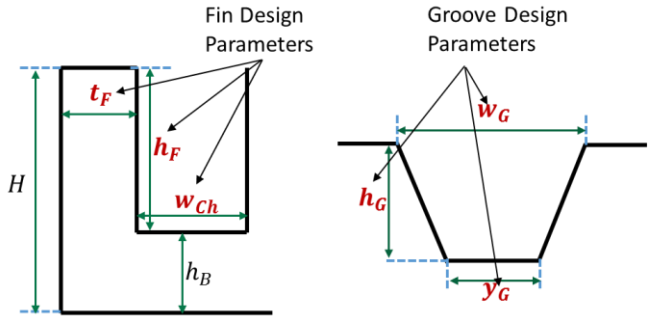

Fig. 8 Fin (Channel) and Groove Design Parameters

Fig. 9 shows the general schematic of the optimized cold-plate, with an exaggeration in fin thickness and channel width, in which the number of fins is equal to the number of channels minus one.

To specify the range of variation of the design parameters, we make the quantities dimensionless. Table 3 illustrates the dimensionless design parameters together with their range of variations. Eqs. (7) and (9) in terms of dimensionless design variables are rewritten as follows:

$$\lambda + \varphi = 1 \tag{10}$$

$$N = \left\lceil \frac{\omega + \alpha}{\alpha + 1} \right\rceil \tag{11}$$

where $\lambda = \frac{h_B}{H}$ and $\omega = \frac{W}{w_{Ch}}$.

It is worth mentioning that, the cross section shape of the baseline groove is trapezoidal because of manufactural reasons. However in the optimization process the groove is triangular for $\delta = 0$, rectangular for $\delta = 1$ and trapezoidal for $0 < \delta < 1$.

Table 3. Dimensionless Design Parameters and Ranges of Variation

Parameters	α	β	φ	σ	δ	γ
Definition	$\frac{t_F}{w_{Ch}}$	$\frac{h_F}{w_{Ch}}$	$\frac{h_F}{H}$	$\frac{h_G}{h_F}$	$\frac{y_G}{w_G}$	$\frac{w_G}{l_2}$
Range of Variation	[0.6 1.2]	[4 12]	[0.6 0.7]	[0.25 1]	[0 1]	[0.1 0.5]

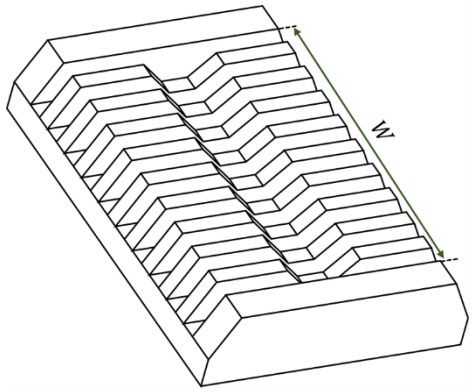

Fig. 9 General Schematic of Optimized Metal Part

Response Parameters

A multi-objective optimization is performed to minimize two response parameters. One of the response parameters that is a measure of thermal performance of the cold-plate is thermal resistance and is defines as:

$$R_{th} = \frac{T_{B,max} - T_{in}}{q''} \tag{12}$$

where q'' symbolizes cold-plate heat flux and $T_{B,max}$ and T_{in} are maximum base and coolant inlet temperatures, respectively.

The other response parameter is hydraulic resistance which is a measure of pressure drop and is defined as:

$$R_h = \frac{\Delta P}{Q} \tag{13}$$

where ΔP is the pressure drop across the channels and Q is coolant volumetric flow rate of the heat sink.

Experimental Design

RSM with face centered central composite design (FCCCD) was used to generate 53 design points in the design space. The response parameters were calculated at these design points using CFD. The results of response parameters associated with channel Reynolds numbers are shown in Table 4. The maximum value of 307.1 for channel Reynolds number confirms that the flow is laminar through the channels.

Regression Function and Analysis of Variance

Table 5 shows the results of a full analysis of variance (ANOVA) for R_{th}. The first column of this table is the degree of freedom (DOF) which is the number of variable levels minus

one. The second column is the adjusted sum of squares (Adj. SS) which is a measure of the variation in the response data that is caused by each term in the regression function. The adjusted

Table 4. Calculated Response Parameters for FCCCD Points

No.	Design Parameters						Re_{D_h}	Response Parameters	
	α	β	φ	γ	δ	σ		$R_{th}(K.mm^2/W)$	$R_h(1/m.s)$
1	0.9	8	0.65	0.3	0.5	0.250	149.8	34.06	16972.32
2	0.9	8	0.65	0.3	0.5	0.625	149.8	34.56	15737.85
3	0.9	8	0.65	0.3	0.5	0.625	149.8	34.56	15737.85
4	0.9	8	0.65	0.3	0.5	0.625	149.8	34.56	15737.85
5	0.9	8	0.65	0.3	0.5	0.625	149.8	34.56	15737.85
6	1.2	12	0.60	0.5	0.0	1.000	119.7	25.73	54117.45
7	0.9	8	0.60	0.3	0.5	0.625	149.7	31.50	28262.00
8	1.2	4	0.70	0.1	1.0	1.000	290.3	71.18	3223.11
9	0.6	4	0.70	0.1	0.0	1.000	224.4	60.21	2578.06
10	1.2	12	0.70	0.5	1.0	1.000	118.6	54.77	13541.92
11	0.6	12	0.60	0.5	1.0	1.000	87.7	46.78	32548.00
12	0.6	4	0.60	0.5	1.0	0.250	225.8	52.12	8148.80
13	0.9	8	0.65	0.3	0.5	0.625	149.8	34.56	15737.85
14	0.6	12	0.60	0.5	0.0	0.250	87.7	25.32	41424.10
15	0.6	4	0.60	0.1	1.0	1.000	225.8	52.01	7508.91
16	0.9	8	0.65	0.3	0.5	1.000	149.8	35.04	15275.74
17	0.6	8	0.65	0.3	0.5	0.625	125.3	33.98	12565.60
18	0.6	4	0.70	0.1	1.0	0.250	224.4	55.61	4307.72
19	0.6	12	0.70	0.1	0.0	0.250	87.6	29.67	18841.34
20	1.2	4	0.60	0.1	1.0	0.250	307.1	51.42	21415.08
21	0.6	12	0.70	0.5	0.0	1.000	87.6	30.31	11206.51
22	1.2	12	0.60	0.5	1.0	0.250	119.7	25.90	52939.90
23	0.9	8	0.65	0.3	0.5	0.625	149.8	34.56	15737.85
24	0.9	8	0.65	0.3	1.0	0.625	149.8	35.09	14652.68
25	0.9	8	0.65	0.1	0.5	0.625	149.8	33.74	16652.83
26	1.2	4	0.70	0.1	0.0	0.250	290.3	51.42	26530.75
27	0.9	8	0.65	0.3	0.5	0.625	149.8	34.56	15737.85
28	1.2	12	0.70	0.5	0.0	0.250	118.6	29.55	18319.69
29	0.6	12	0.6	0.1	0.0	1.000	87.7	24.60	52369.97
30	0.9	8	0.65	0.5	0.5	0.625	149.8	35.79	13433.69
31	0.6	4	0.70	0.5	1.0	1.000	224.4	90.48	2379.04
32	0.6	4	0.70	0.5	0.0	0.250	224.4	60.54	3812.02
33	0.6	12	0.70	0.5	1.0	0.250	87.6	30.35	11035.60
34	0.6	12	0.70	0.1	1.0	1.000	87.6	28.79	12376.84
35	1.2	4	0.60	0.5	0.0	0.250	307.1	52.88	17568.37
36	1.2	12	0.60	0.1	0.0	0.250	119.7	24.44	89471.13
37	0.9	8	0.70	0.3	0.5	0.625	148.2	38.61	8527.40
38	0.6	4	0.60	0.1	0.0	0.250	225.8	46.53	19450.00
39	0.9	8	0.65	0.3	0.5	0.625	149.8	34.56	15737.85
40	0.9	8	0.65	0.3	0.5	0.625	149.8	34.56	15737.85
41	0.9	4	0.65	0.3	0.5	0.625	258.4	60.43	6753.84
42	1.2	4	0.70	0.5	1.0	0.250	290.4	68.43	4401.63
43	1.2	4	0.60	0.1	0.0	1.000	307.1	55.26	16138.94
44	1.2	12	0.70	0.1	0.0	1.000	118.6	28.82	20177.00
45	0.6	12	0.60	0.1	1.0	0.250	87.7	24.68	53901.15
46	0.9	12	0.65	0.3	0.5	0.625	103.7	26.62	30441.48
47	1.2	4	0.60	0.5	1.0	1.000	307.1	77.08	11860.37
48	0.6	4	0.60	0.5	0.0	1.000	225.8	53.62	8298.08
49	1.2	12	0.70	0.1	1.0	0.250	118.6	28.92	22345.54
50	1.2	12	0.60	0.1	1.0	1.000	119.7	24.54	71416.93
51	1.2	4	0.70	0.5	0.0	1.000	290.3	72.47	4607.67
52	1.2	8	0.65	0.3	0.5	0.625	172.3	35.84	18862.94
53	0.9	8	0.65	0.3	0.0	0.625	149.8	34.20	16478.88

mean square (Adj. MS) is calculated by dividing the adjusted sum of squares by their corresponding degrees of freedom. The F-value is defined as the ratio of the mean regression sum of squares to the mean error sum of squares and is a non-negative real number. The higher F-value a term has in a regression function, the more significant effect it has on the response. In the last column, the P-value is the probability of rejecting the null hypothesis when it is true. In an ANOVA regression table, terms with P-values larger than 0.1 do not have substantial effect on the response parameter and should be rejected in the regression function. As it can be seen in Table 5, α, all square terms except β^2 and many interaction terms have P-values larger than 0.1 and should be neglected. R^2 is the ratio of the sum of squares due to regression (SSR) to sum of squared errors (SSE) and is called coefficient of determination. $R^2$and Adj. R^2 usually are the criteria of the fitness quality. The closer $R^2$and Adj. R^2 are to one, the more accurate the regression function predicts. More details about regression and ANOVA analysis is available in [15].

Table 5. ANOVA Full Table for Thermal Resistance (R_{th})

Source	DOF	Adj. SS	Adj. MS	F-Value	P-Value
Model	27	1.23373	0.045694	34.83	0.000
Linear	6	1.01118	0.168531	128.45	0.000
α	1	0.00321	0.003213	2.45	0.130
β	1	0.80112	0.801117	610.59	0.000
φ	1	0.05418	0.054176	41.29	0.000
γ	1	0.05788	0.057878	44.11	0.000
δ	1	0.03728	0.037277	28.41	0.000
σ	1	0.05752	0.057524	43.84	0.000
Square	6	0.13923	0.023205	17.69	0.000
α^2	1	0.00006	0.000059	0.04	0.834
β^2	1	0.01980	0.019795	15.09	0.001
φ^2	1	0.00010	0.000098	0.07	0.787
γ^2	1	0.00003	0.000029	0.02	0.882
δ^2	1	0.00001	0.000013	0.01	0.922
σ^2	1	0.00000	0.000004	0.00	0.954
2-Way Interaction	15	0.08332	0.005555	4.23	0.001
$\alpha\beta$	1	0.00225	0.002253	1.72	0.202
$\alpha\varphi$	1	0.00020	0.000201	0.15	0.699
$\alpha\gamma$	1	0.00004	0.000036	0.03	0.870
$\alpha\delta$	1	0.00042	0.000424	0.32	0.575
$\alpha\sigma$	1	0.00069	0.000695	0.53	0.474
$\beta\varphi$	1	0.00788	0.007885	6.01	0.022
$\beta\gamma$	1	0.00276	0.002762	2.11	0.159
$\beta\delta$	1	0.00114	0.001141	0.87	0.360
$\beta\sigma$	1	0.00716	0.007155	5.45	0.028
$\varphi\gamma$	1	0.00217	0.002166	1.65	0.211
$\varphi\delta$	1	0.00117	0.001175	0.90	0.353
$\varphi\sigma$	1	0.00215	0.002147	1.64	0.213
$\gamma\delta$	1	0.01965	0.019647	14.97	0.001
$\gamma\sigma$	1	0.01685	0.016850	12.84	0.001
$\delta\sigma$	1	0.01878	0.018784	14.32	0.001
Error	25	0.03280	0.001312	–	–
Lack- of -Fit	17	0.03280	0.001929	–	–
Pure Error	8	0.00000	0.000000	–	–
Total	52	1.26654	–	–	–

Standard Deviation	R^2	R^2(Adjusted)	R^2(Predicted)
0.0348366	97.41%	94.61%	78.34%

The backward-elimination process to estimate the regression function eliminates terms which are not significant (P-value> 0.1). The regression function of R_{th} based on backward-elimination is given by Eq. (14) and the corresponding ANOVA results are presented in Table 6.

$$R_{th} = 7.50 - 8.77\beta + 142.60\varphi - 10.88\gamma - 8.89\delta + 3.30\sigma + 0.67\beta^2 - 7.85\beta\varphi - \beta\sigma + 24.78\gamma\delta + 30.60\gamma\sigma + 12.92\delta\sigma \quad (14)$$

In Table 6, all insignificant terms with P-values larger than 0.1 are eliminated. The values of R^2 and Adj. R^2 are 96.09% and 95.02%, respectively. Since, these values are close to unity and the difference between them is small enough, the achieved regression function provides a precise relationship between the design parameters and thermal resistance. However, to have a more-detailed view on how this polynomial works, we can perform a regression diagnostics and detect the regression model violations. To do this, we have to check for the following assumptions:

1- Linearity assumption: Standard multi-regression can estimate the relation between design and response parameters accurately when it is linear in nature.
2- Normality assumption: The errors of the regression function should have a normal distribution. Highly skewed residuals can be a symptom of a low quality fitting.
3- Homoscedasticity (constant variance) assumption: It means that the variance of errors is constant and does not depend on their mean.

Table 6. ANOVA Backward-Elimination Table for Thermal Resistance (R_{th})

Source	DOF	Adj. SS	Adj. MS	F-Value	P-Value
Model	11	1.21678	0.110616	91.15	0.000
Linear	5	1.00797	0.201594	166.11	0.000
β	1	0.80112	0.801117	660.12	0.000
φ	1	0.05418	0.054176	44.64	0.000
γ	1	0.05788	0.057878	47.69	0.000
δ	1	0.03728	0.037277	30.72	0.000
σ	1	0.05752	0.057524	47.40	0.000
Square	1	0.13849	0.138487	114.11	0.000
β^2	1	0.13849	0.138487	114.11	0.000
2-Way Interaction	5	0.07032	0.014064	11.59	0.000
$\beta\varphi$	1	0.00788	0.007885	6.50	0.015
$\beta\sigma$	1	0.00716	0.007155	5.90	0.020
$\gamma\delta$	1	0.01965	0.019647	16.19	0.000
$\gamma\sigma$	1	0.01685	0.016850	13.88	0.001
$\delta\sigma$	1	0.01878	0.018784	15.48	0.000
Error	41	0.04976	0.001214	–	–
Lack- of -Fit	33	0.04976	0.001508	–	–
Pure Error	8	0.00000	0.000000	–	–
Total	52	1.26654	–	–	–

Standard Deviation	R^2	R^2(Adjusted)	R^2(Predicted)
0.0348366	96.09%	95.02%	91.82%

In addition to the above assumptions the regression model should also be checked for outliers and influential points.

In order to check the linearity, normality and homoscedasticity assumptions the standard residual plots of thermal resistance are shown in Fig. 10. The normal probability plot displays normal scores (what is expected to be obtained when a sample of size n is taken from a standard normal distribution.) versus standardized residuals. If the residuals have a normal distribution, this plot resembles an almost straight line [15]. From this plot, the normality assumption of the regression model is satisfied. From the standardized residuals versus fitted values, both the linearity and homoscedasticity assumptions are checked. With a random scatter of points, we can conclude that the linearity assumption holds. As the second diagram of Fig. 10 shows no trend is distinguishable for the points so that there should not be any problem associated with the linearity of our regression model. A funnel-shape distribution for residual trend, either diverging or converging with the fitted values, is a sign of heterogeneity of variance. In the standardized residuals versus fitted values plot we witness a roughly horizontal band around the line of zero which implies the consistency of variance. The skewness of the data can be determined from the standardized residuals histogram [16]. As it can be seen in the histogram, the residuals distribution is not remarkably skewed however it is not entirely symmetric. Points with absolute standardized residuals higher than 2 or more than 3 times of standard deviation far from the mean are recognized as the outliers [15]. From either the fitted value or histogram diagrams, we find that there is at least one outlier in our data (No 26 in Table 4). In a regression model a point is said to be an influential point provided that its deletion, singly or together with two or three others, changes the fitted relation considerably. In order to specify the influential points, a measure proposed by Cook [17] named Cook's distance was used. Cook's distance of the regression function of Eq. 14 is plotted in Fig. 11. A point is classified as an influential point if it satisfies the inequality of:

$$Cook's\ distance > 1 \qquad (15)$$

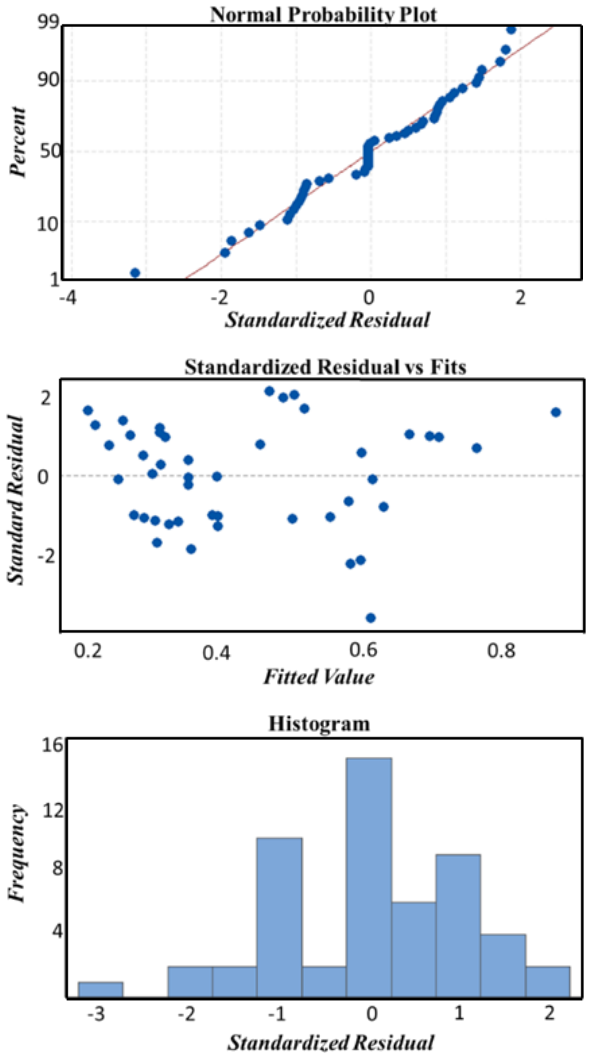

Fig. 10 Residual Plots of Thermal Resistance

Although as Fig. 11 shows the point number 26 has a high value of leverage (Cook's distance) in comparison to the other points (greater than 0.4), it does not satisfy the inequality of Eq. (15). Consequently, the point number 26 cannot be recognized as an influential point. The same analysis completed for thermal resistance can be done for hydraulic resistance.

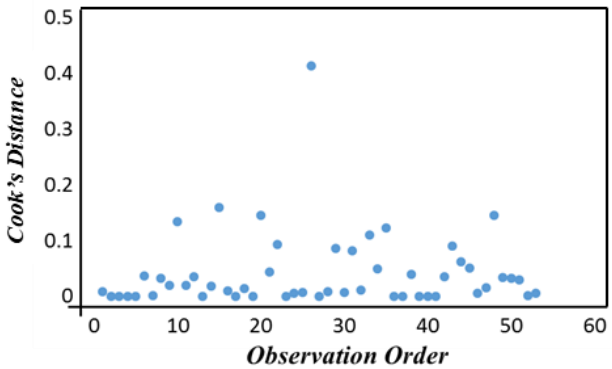

Fig. 11 Cook's Distance Criterion

Transformation

In order to improve the accuracy of the regression models, logarithmic transformation was used for both thermal and hydraulic resistances. Although the logarithmic transformation increases the normality and decreases the effects of outliers, it is mainly used to increase the data linearity and remove heteroscedasticity. Therefore, it makes the regression model more accurate.

While in this study, for both thermal and hydraulic resistances, the linearity of data is not the major problem, more accurate results were obtained by applying logarithmic transformation. For example, the average error of thermal resistance decreased from about 6.5% to 5.4% and the number of points with errors larger than 10% decreased from 14 to 5.

$$\bar{R}_{th} = ln(R_{th}) \tag{16}$$

$$\bar{R}_h = ln(R_h) \tag{17}$$

Replacing R_{th} and R_h with the new response parameters $\bar{R}_{th}$ and $\bar{R}_h$ in Table 4 and applying the backward-elimination analysis of variance we approach the new ANOVA results shown in Tables 7 and 8. The corresponding regression relations are given in Eqs. (18) and (19).

$$\begin{aligned} R_{th} = exp(&3.8340 - 0.2761\beta + 1.7390\varphi - \\ &0.2370\gamma - 0.1877\delta - 0.1118\sigma + \\ &0.0117\beta^2 + 0.5210\gamma\delta + 0.6380\gamma\sigma + \\ &0.2596\delta\sigma) \end{aligned} \tag{18}$$

$$\begin{aligned} R_h = exp(&13.61 + 1.20\alpha + 0.32\beta - 7.53\varphi - \\ &1.74\gamma - 0.69\delta + 0.34\sigma - 0.05\alpha\beta - \\ &0.26\beta\varphi + 0.03\beta\delta + 0.70\beta\sigma - 2.96\varphi\sigma + \\ &1.39\gamma\sigma + 0.27\delta\sigma) \end{aligned} \tag{19}$$

Table 7. ANOVA Backward-Elimination Table for $\bar{R}_{th}$

Source	DOF	Adj. SS	Adj. MS	F-Value	P-Value
Model	9	5.87581	0.65287	116.09	0.000
Linear	5	5.21582	1.04316	185.49	0.000
β	1	4.36126	4.36126	775.50	0.000
φ	1	0.25691	0.25691	45.68	0.000
γ	1	0.24245	0.24245	43.11	0.000
δ	1	0.14536	0.14536	25.85	0.000
σ	1	0.20984	0.20984	37.31	0.000
Square	1	0.42406	0.42406	75.41	0.000
β^2	1	0.42406	0.42406	75.41	0.000
2-Way Interaction	3	0.23593	0.07864	13.98	0.000
$\gamma\delta$	1	0.08674	0.08674	15.42	0.000
$\gamma\sigma$	1	0.07335	0.07335	13.04	0.001
$\delta\sigma$	1	0.07583	0.07583	13.48	0.001
Error	43	0.24182	0.00562	–	–
Lack- of -Fit	35	0.24182	0.00691	–	–
Pure Error	8	0.00000	0.00000	–	–
Total	52	6.11763	–	–	–

Standard Deviation	R^2	R^2(Adjusted)	R^2(Predicted)
0.0749918	96.05%	95.22%	92.93%

Comparing Tables 6 and 7 (thermal resistance regression models with and without logarithmic transformation), there is no significant changes in R^2s and Adj. R^2; however, we have a slight increase in R^2 (predicted) which confirms more precise prediction of Eq. (18) than Eq. (14). The standard residual plots of the Eqs. (18) and (19) were very similar to those of Eq. (14) and were not given here to prevent unnecessary repetition.

Table 8. ANOVA Backward-Elimination Table for $\bar{R}_h$

Source	DOF	Adj. SS	Adj. MS	F-Value	P-Value
Model	13	32.3409	2.4878	105.58	0.000
Linear	6	31.1232	5.1872	220.15	0.000
α	1	1.9609	1.9609	83.22	0.000
β	1	15.3187	15.3187	650.13	0.000
φ	1	11.1729	11.1729	474.18	0.000
γ	1	1.0256	1.0256	43.53	0.000
δ	1	0.5706	0.5706	24.22	0.000
σ	1	1.0745	1.0745	45.60	0.000
2-Way Interaction	7	1.2177	0.1740	7.38	0.000
$\alpha\beta$	1	0.1136	0.1136	4.82	0.034
$\beta\varphi$	1	0.0870	0.0870	3.69	0.062
$\beta\delta$	1	0.1373	0.1373	5.83	0.021
$\beta\sigma$	1	0.3557	0.3557	15.10	0.000
$\varphi\sigma$	1	0.0983	0.0983	4.17	0.048
$\gamma\sigma$	1	0.3457	0.3457	14.67	0.000
$\delta\sigma$	1	0.0800	0.0800	3.40	0.073
Error	39	0.9189	0.0236	–	–
Lack- of -Fit	31	0.9189	0.0296	–	–
Pure Error	8	0.0000	0.0000	–	–
Total	52	33.2599	–	–	–

Standard Deviation	R^2	R^2(Adjusted)	R^2(Predicted)
0.153501	97.24%	96.32%	92.52%

In addition to statistical validation the accuracy of the regression functions (Eqs. (18) and (19)) was proved numerically. Two intermediate points were selected from the design parameters range of variation, shown in Table 3, and the results of CFD modeling are compared with regression model predictions in Table 9.

Table 9. Results of Regression Confirmation by CFD

Design Parameters						$R_{th}(K.mm^2/W)$			R_h $(1/m.s)$		
α	β	φ	γ	δ	σ	Simulation	Regression	Error	Simulation	Regression	Error
1.050	10.0	0.65	0.20	0.25	0.4375	28.12	29.46	4.56%	29683.32	27509.73	7.90%
0.625	4.5	0.60	0.40	0.00	1.0000	48.40	50.38	4.10%	9917.75	9707.64	2.12%

It is worth mentioning that both Eqs. (14) and (18) do not include the design parameter α which implies that in the range of variation selected for this parameter, the thermal resistance of the heat sink is not affected by fin thickness remarkably. Although making the fins thinner increases their thermal resistance, it simultaneously increases the total convective heat transfer surface area and vice versa.

Sensitivity Analysis

Sensitivity analysis is a method to determine how the uncertainties in independent variables (design parameters) affect dependent variables (response parameters). By using sensitivity analysis, the effective parameters are ranked in order of influence. This analysis can be done both by taking partial derivatives of regression functions with respect to independent variables or using F-values in the analysis of variance results. In the current work we used the second method. The contribution bar chart for thermal and hydraulic resistances is given in Fig. 12. Note that β (channels aspect ratio) has the most significant contributions of 74.2% and 47.4%, respectively. This is in agreement with previous researchers' results for parallel channels where narrower and deeper channels provide lower thermal resistance and pressure drop [10, 18]. Apart from β, it can be seen that φ also has significant effect on hydraulic resistance. The reason is that by increasing the depth of the channels, regardless of their width, we increase their hydraulic diameter, leading to lower pressure drop. There are two conclusions for this sensitivity analysis:

1- The groove geometry is not of great importance for both thermal and hydraulic resistances.
2- Channel height and width are the most influential parameters on the heat transfer performance and pressure drop of the heat sink.

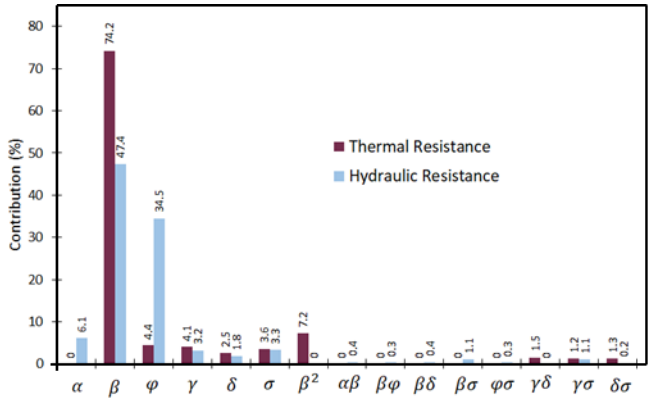

Fig. 12 The Sensitivity Analysis of Design Parameters

Objective Function

The objective function of the optimization is considered as a weighted combination of our response parameters.

$$\Xi = w_{th}(m)\left(\frac{\bar{R}_{th}}{\bar{R}_{th}^{min}}\right) + w_h(m)\left(\frac{\bar{R}_h}{\bar{R}_h^{min}}\right) \qquad (20)$$

where $\bar{R}_{th}^{min}$ and $\bar{R}_h^{min}$ are the minimum values of the regression functions of Eqs. (18) and (19). $w_{th}(m)$ and $w_h(m)$ are the weight factors assigned to thermal and hydraulic resistances.

$$\begin{cases} w_{th}(m) = \frac{m}{10} \\ w_h(m) = \frac{10-m}{10} \end{cases} \qquad m = 0, 1, 2, \dots, 10 \qquad (21)$$

Optimal Designs

The optimal designs were obtained by minimizing the objective function (Ξ) for $m = 0$ to $m = 10$ using the JAYA optimization algorithm [19]. By selecting low values of m we emphasize minimizing hydraulic resistance and with large values of m thermal resistance. The results of this optimization are given in Table 10.

Table 10. Optimization Results

m	w_{th}	w_h	α	β	φ	γ	δ	σ	$R_{th}(K.mm^2/W)$	$R_h\ (1/m.s)$	N
0	0.0	1.0	0.60	4.00	0.70	0.50	1.00	1.00	95.07	1825.85	22
1	0.1	0.9	0.60	4.00	0.70	0.50	1.00	1.00	95.07	1825.85	22
2	0.2	0.8	0.60	4.00	0.70	0.10	1.00	1.00	65.75	1992.02	22
3	0.3	0.7	0.60	4.20	0.70	0.10	1.00	1.00	63.39	2067.10	23
4	0.4	0.6	0.60	6.93	0.70	0.10	1.00	1.00	42.53	4025.08	38
5	0.5	0.5	0.60	9.28	0.70	0.50	1.00	0.25	35.32	5631.89	51
6	0.6	0.4	0.60	10.29	0.70	0.10	1.00	0.25	28.18	9911.00	56
7	0.7	0.3	0.60	10.84	0.70	0.10	1.00	0.25	27.72	10651.97	59
8	0.8	0.2	0.60	11.14	0.60	0.10	1.00	0.25	23.16	33863.74	94
9	0.9	0.1	0.60	11.53	0.60	0.10	1.00	0.25	23.05	35982.93	97
10	1.0	0.0	0.60	11.84	0.60	0.10	1.00	0.25	23.02	37771.12	100

Fig. 13 shows the optimized points together with the RSM design points and the baseline point in a $R_h - R_{th}$ plane. This provides a visual perception of the optimized points.

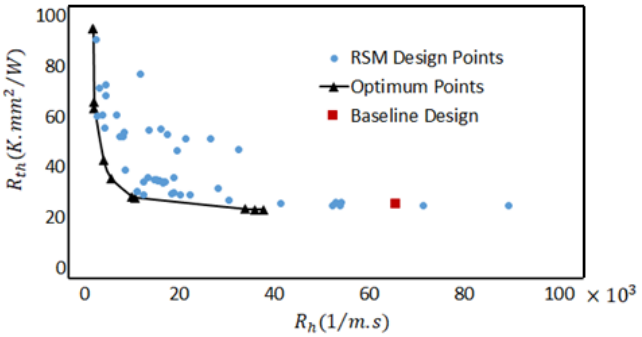

Fig. 13 Baseline, Design and Optimum Points

EFFECT OF GROOVE GEOMETRY ON TEMPERATURE DISTRIBUTION

As shown in Fig. 12, γ, which is the width of the groove to the length of a channel, does not have a significant effect on thermal resistance. However, the temperature contours show that γ has considerable effect on the temperature distribution of the base and the electrical chip. In Fig. 14, the temperature profile along the fin symmetry plane for two similar design points in Table 4 with different γ's (points 11 and 50) are compared. For the narrow-groove design (50), the maximum base (chip) temperature occurs around the channel end (chip edge) as the coolant temperature increases along the channel.

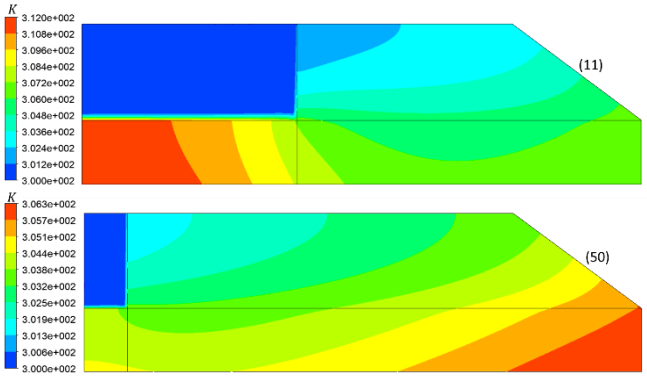

Fig. 14 Temperature Profile for Two Design Points: (11) and (50)

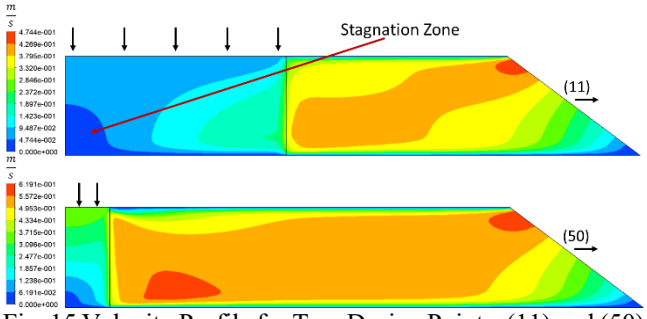

Fig. 15 Velocity Profile for Two Design Points: (11) and (50)

However, for the wide-groove design (11), the maximum temperature occurs around the beginning of the channel (chip center). Compare to narrow grooves, wide grooves create a large stagnation zone in the beginning of the channel where heat

is transferred mainly by diffusion. Fig. 15 compares the velocity profiles on the symmetry plane of the channel for these two design points.

CONCLUSION AND SUMMARY

An impinging flow, warm water-cooled heat sink was modeled and optimized using CFD and RSM. Designed points were modeled and solved numerically. RSM in conjunction with logarithmic transformation were used to generate the regression function. The validity of the regression model was evaluated both statistically and numerically. Sensitivity analysis shows that the channel aspect ratio is the most influential parameter for thermal and hydraulic resistances. The objective function was written as a weighted combination of response parameters. Optimum designs were obtained for different weight factors using the JAYA algorithm. Finally, it was shown that although groove geometry does not have significant effect on our response parameters, it can affect the temperature profile of the base and electrical die.

ACKNOWLEDGEMENT

This work is supported by NSF IUCRC Award No. IIP-1738793. Authors would like to acknowledge M. Seymour and Dr K. Nemati from Future Facilities, S. Schon from QuantaCool, R. Tipton from Emerson and Dr M. S. Tootooni from Mayo Clinic for their useful comments and guidance through the course of this study.

REFERENCES

[1] Subasi, B. Sahin and I. Kaymaz, "Multi-Objective Optimization of a Honeycomb Heat Sink Using Response Surface Method," International Journal of Heat and Mass Transfer, vol. 101, pp. 295-302, 2016.

[2] R. V. Rao, K. C.m More, J. Taler and P. Oclon, "Dimensional Optimization of a Micro-Channel Heat Sink Using JAYA Algorithm," Applied Thermal Engineering, vol. 103, pp. 572-582, 2016.

[3] C. Chou, N. M. Liu, J. T. Horng and K. T. Chiang, "Designing Parameter Optimization of a Parallel-Plain Fin Heat Sink Using the Grey-Based Fuzzy Algorithm with the Orthogonal Arrays," International Journal of Thermal Science, vol. 48, pp. 2271-2279, 2009.

[4] K. T. Chiang, C. C. Chou and N. M. Liu, "Application of Response Surface Methodology in Describing the Thermal Performances of a Pin-Fin Heat Sink," International Journal of Thermal Science, vol. 48, pp. 1196-1205, 2009.

[5] K. Kulkarni, A. Afzal and K. Y. Kim, "Multi-Objective Optimization of a Double-Layered Microchannel Heat Sink with Temperature-Dependent Fluid Properties," Applied Thermal Engineering, vol. 99, pp. 262-272, 2016.

[6] K. T. Chiang, "Optimization of the Design Parameters of Parallel-Plain Fin Heat Sink Module Cooling Phenomenon Based on the Taguchi Method," International Communications in Heat and Mass Transfer, vol. 32, pp. 1193-1201, 2005.

[7] Y. T. Yang, S. C. Lin, Y. H. Wang and J. C. Hsu, "Numerical Simulation and Optimization of Impinging Cooling for Rotating and Stationary Pin-Fin Heat Sinks," International Journal of Heat and Fluid Flow, vol. 44, pp. 383-393, 2013.

[8] S. Manivannan, S. P. Prasanna, R. Arumugam and N. M. Sudharsan, "Multi-Objective Optimization of Flat Plate Heat Sink Using Taguchi-Based Grey Relational Analysis," International Journal of Advanced Manufacturing Technology, vol. 52, pp. 739-749, 2011.

[9] L. Lin, Y. Y. Chen, X. X. Zhang, and X. D. Wang, "Optimization of Geometry and Flow Rate Distribution for Double-Layer Microchannel Heat Sink," International Journal of Thermal Science, vol. 78, pp. 158-168, 2014.

[10] X. L. Xie, Z. J. Liu, Y. L. He and W. Q. Tao, "Numerical Study of Laminar Heat Transfer and Pressure Drop Characteristics in a Water-Cooled Minichannel Heat Sink," Applied Thermal Engineering, vol. 29, pp. 64-74, 2009.

[11] R. H. Myers. D. H. Montgomery and C. M. Anderson-Cook, "*Response Surface Methodology,*" 4th Edition, John Wiley & Sons, New Jersey, USA, 2016.

[12] Y. S. Muzychka and M. M. Yovanovich, "Pressure Drop in Laminar Developing Flow in Noncircular Ducts: A Scaling and Modeling Approach," Journal of Fluids Engineering, vol. 131, 111105 (11 pages), 2009.

[13] http://www.coolitsystems.com

[14] Y. Hadad, B. Ramakishnan, S. Alkharabsheh, P. Chiarot and B. Sammakia, "Numerical Modeling and Optimization of a V-Groove Warm Water Cold-Plate," 33rd SEMI-THERM Symposium, IEEE, San Jose, California, USA, 2017.

[15] S. Chatterjee and A. S. Hadi, "*Regression Analysis by Example,*" 5th Edition, John Wiley & Sons, New Jersey, USA, 2012.

[16] N. Zheng, P. Liu, Z. Liu, W. Liu, "Numerical Simulation and Sensitivity Analysis of Heat Transfer Enhancement in a Flat Heat Exchanger Tube with Discrete Inclined Ribs," International Journal of Heat and Mass Transfer, vol. 112, pp. 509-302, 520, 2017.

[17] R. D. Cook, "Detection of influential observation in linear regression," Technometrics, vol 19, pp. 15-18, 1977.

[18] H. R. Upadhye, S. G. Kandlikar, "Optimization of Microchannel Geometry for Direct Chip Cooling Using Single Phase Heat Transfer" Microchannels and Minichannels, ASME, Rochester, New York, USA, 2004.

[19] R. V. Rao, "JAYA: A Simple and New Optimization Algorithm for Solving Constrained and Unconstrained Optimization Problems," International Journal of Industrial Engineering Computation, vol. 7, pp. 19-34, 2016.